HIBP study of Alfvén Eigenmodes Properties and Dynamics in the TJ-II Stellarator

L.G. Eliseev 1), A.V. Melnikov 1), R. Jiménez-Gómez 2), E. Ascasibar 2), A. Alonso 2), A.A. Chmyga 3), C. Hidalgo 2), A.D. Komarov 3), A.S. Kozachek 3), I.A. Krasilnikov 1), L.I. Krupnik 3), S.M. Khrebtov 3), A. Könies 4), Yu.K. Kuznetsov 5), M. Liniers 2), S.E. Lysenko 1), V.A. Mavrin 1), J.L. de Pablos 2), M.A. Pedrosa 2), S.V. Perfilov 1), A.I. Smolyakov 6), D. Spong 7), M.V. Ufimtsev 8), T. Ido 9), K. Nagaoka 9), S. Yamamoto 10), and A.I. Zhezhera 3)

1) Institute of Tokamak Physics, RRC "Kurchatov Institute", 123182, Moscow, Russia,
2) Asociación EURATOM-CIEMAT, 28040, Madrid, Spain,
3) Institute of Plasma Physics, NSC KIPT, 61108, Kharkov, Ukraine,
4) Max-Planck-Institut für Plasmaphysik, EURATOM-Association, D-17491, Greifswald, Germany,
5) Institute of Physics, University of Sao Paulo, 05508-090, Brazil,
6) University of Saskatchewan, 116 Science Place, Saskatoon SK S7N 5E2, Canada,
7) Oak-Ridge NL, Tennessee, USA,
8) Department of Computational Mathematics and Cybernetics, Moscow State University, Russia,
9) National Institute for Fusion Science, 322-6 Oroshi-cho, Toki 509-5292, Japan,
10) Institute of Advanced Energy, Kyoto University, Kyoto, 611-0011, Japan.

E-mail contact of main author: melnik@nfi.kiae.ru

Abstract. Energetic ion driven Alfvén Eigenmodes (AEs) in the NBI-heated plasma at the TJ-II stellarator were studied by Heavy Ion Beam Probing (HIBP) in the core, and by Langmuir (LP) and Mirnov probes (MP) at the edge. HIBP observed the locally (~1 cm) resolved AE at radii $-0.8 < \rho < 0.9$. A set of AE branches with low poloidal numbers (m<8) was detected by HIBP and MP. AEs on the density, electric potential and poloidal magnetic field oscillations were detected by HIBP at frequencies 50 kHz < f_{AE} < 300 kHz. The LP, MP and HIBP data have a high coherency for specific branches of AE. When the density rises due to NBI fueling, AE frequency decreases in accordance to the Alfven law $f_{AE} \sim n_e^{-1/2}$, but the AE phase characteristics, such as cross-phases between the B_{pol}, n_e and potential oscillations remains unchanged. With the f_{AE} decrease, the AE poloidal rotation velocity remains the same due to an accompanying decrease in k_θ. Comparison with computational MHD mode predictions indicates that some of the more prominent frequency branches can be identified as radially extended HAE (helical) modes coupled to GAE (global) modes. AEs present quite pronounced quasi-coherent peaks in the turbulent particle flux spectra. AEs may contribute to both outward and inward flux, and also produce no flux, depending on the phase relations between E_{pol} and n_e oscillations.

1. Introduction

Energetic ion driven Alfvén Eigenmodes (AEs) are believed to be an important element affecting the transport of fast particles in a future reactor. The study of the properties of the AEs in modern toroidal devices is a crucial contribution to reactor relevant physics. AEs are conventionally studied by Mirnov probes, which provide the poloidal m and toroidal n mode numbers and their spectral characteristics [1]. Recently Heavy Ion Beam Probing (HIBP) has been developed as a new tool to study AEs with high spatial and frequency resolution [2]. HIBP in the TJ-II heliac has observed AEs with good local resolution (~1 cm) at radii $-1 < \rho < 1$. This report presents new observations of the phenomenology and features of the NBI induced AEs in TJ-II and the results of the computer modelling performed to identify the most pronounced AEs, observed in TJ-II so far.

2. Experimental set-up and HIBP diagnostics

TJ-II is a four-field-period low-magnetic shear stellarator with helical axis and the following parameters: B_{tor} = 1 T, $<R>$ = 1.5 m, $<a>$ = 0.22 m, $\overline{n_e}$ = (0.3 – 6)×10^{19} m^{-3}. TJ-II operates with two gyrotrons with total power up to P_{ECRH} = 300 kW each, combined with two neutral beam injectors (NBI) that accelerate 30 kV H^0 beams with a total injected port through power of up to P_{NBI} = 400-450 kW each. The "Co-" injector is directed along the toroidal field of the device. Its operation leads to an increase of the vacuum rotational transform. The "Counter-" injector is directed opposite to the toroidal field. Its operation leads to a decrease of the rotational transform. HIBP in TJ-II operates with Cs^+ ions, E_b = 125 keV [3]. It is able to study directly the plasma electric potential φ and density n_e with a good spatial (< 1 cm) and temporal (1 μs) resolution. The crucial element of the present HIBP operation is the two-slit energy analysis of secondary ions, which allows us to observe two detector grids simultaneously. Two sample volumes are optimized to be separated poloidaly to find the poloidal component of the electric field E_{pol} by the difference in local potentials, $E_{pol} =(\varphi_1-\varphi_2)/x$, x~1 cm. This limits the poloidal wave vector, $k_\theta < 2$ cm^{-1}. The radial $E\times B$ drift velocity is $V_r = E_{pol}/B_{tor}$. Finally, the radial turbulent particle flux is $\boldsymbol{\Gamma_r}(t) = \tilde{n}_e\tilde{V}_r = 1/B_{tor}\, \tilde{n}_e(t)\, \tilde{E}_{pol}(t) = \boldsymbol{\Gamma_{E\times B}}$ was extracted in the bulk plasma for the first time in stellarators [4]. To measure $\boldsymbol{\Gamma_{E\times B}}(t)$, the density fluctuations $\tilde{n}_e$ should be obtained simultaneously at the same position as $\tilde{E}_{pol}$ that is provided by combined potentials and beam current measurements with HIBP. For the analysis of the flux dynamics in arbitrary units, or for frequency spectra analysis, the relative data for density oscillations $\delta n_e(t) = \tilde{I}_t(t)/\overline{I_t}$ is sufficient. In the low-density case, for the estimation of the absolute value of $\boldsymbol{\Gamma_{E\times B}}(t)$, $\tilde{n}_e$ may be replaced by $\tilde{I}_t(t)$. In the higher-density case, one should take into account the attenuation effect by the expression: $\tilde{n}_e = \tilde{I}_t/\overline{I_t}\cdot\overline{n}_e$, where oscillatory component $\tilde{I}_t/\overline{I_t}$ is measured by HIBP, and normalization factor $\overline{n_e}$ is provided by other diagnostics like interferometry.

3. Mode observations

Typically the NBI-induced AEs are not visible as single frequency oscillations, but as a variety of the quasi-monochromatic peaks, excited simultaneously in TJ-II plasmas. The set of low m (m<8) branches, detected with high frequency resolution (< 5 kHz) is expected to represent different types of AEs. The typical example of the AEs temporal evolution is presented in Figure 1. Oscillations in the AE frequency range are observed in the local density, electric potential and poloidal magnetic field, simultaneously detected by HIBP in the frequency range 50 kHz< f_{AE} <300 kHz. AEs are visible in the NBI-heated plasma; a high coherency between Mirnov probes and HIBP data was found for specific branches of AE. The mode location is close to the plasma center for co-NBI (<450 kW), and near the mid-radius for counter- (<450 kW) and balanced NBI (<900 kW), indicating a deformation of the rotational transform profile by NBI driven current. When the density rises, the AE frequency decreases, f_{AE}~$n_e^{-1/2}$; however, the cross-phases between the density and potential, density and poloidal magnetic field oscillations remain constant.

4. Mode features

The existence of high correlations was reported in the earlier papers [2, 5] between plasma potential, density and B_{pol}, as measured by HIBP. It was also found that high correlations were present between the core density measured by HIBP and MP signals. It is a remarkable feature of the measurements of the E_{pol}, induced by AEs. Some of the modes present core-

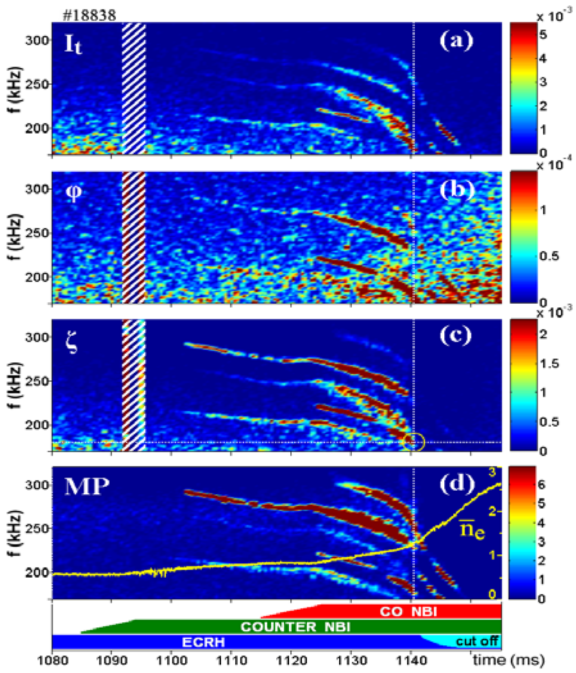

FIG. 1. PSD time evolution of HIBP (ρ = 0.5) and Mirnov probe signals. Alfvén Eigenmodes are pronounced:
(a) on the total secondary beam current I_t proportional to n_e;
(b) on the potential φ;
(c) on the toroidal shift of secondary beam ζ proportional to B_{pol};
(d) on the Mirnov probe signal. The line-averaged density is also shown in (d). Instrumental gap in HIBP signal is shown by hatched ribbons in (a, b, c). The AEs amplitudes increase and new mode branches appear after the co-NBI start owing to iota variation by NBI current drive. Yellow circle marks the modeled mode, presented in Fig. 8.

edge (long range) radial correlations between E_{pol}, measured by HIBP in the core and $E_{pol}^{LP} = (\varphi_1\text{-}\varphi_2)^{\text{floating}}/x^{LP}$, x^{LP}~3 mm. Note, the LP measured poloidal wave vector, $k_\theta^{LP} < 10$ cm^{-1}. Figure 2 presents an example of the core-edge correlations.

5. Poloidal mode number determination

Simultaneous poloidally resolved measurements provide sufficient data to extract the poloidal mode number m by the cross-phase of two separated signals. To estimate the temporal evolution of the link between the data $x(t)$ and $y(t)$ from various signals one should calculate the coherency Coh_{xy} and cross-phase θ_{xy} spectrograms, which are produced by auto-power $S_{xx}(f, t)$ and cross-power $S_{xy}(f, t)$ Fourier spectrograms:

$$Coh_{xy}(f, t) = |S_{xy}| \,/\, |S_{xx}\, S_{yy}|^{1/2}, \qquad \theta_{xy}(f, t) = \tan^{-1} \{\text{Im}\,(S_{xy}) \,/\, \text{Re}(S_{xy})\} \qquad (1)$$

For the poloidally propagated density perturbations one should use the $S_{xy}(f, t) = S_{1,2}^{Itot}(f, t)$– spectrogram for two signals of the total beam current I_{tot}, that provides the $\theta_{n1\,n2}$ cross-phase between the densities, measured in two sample volumes [2]. The poloidal wave vector and mode number are obtained from

$$k_\theta = \theta_{n1\,n2} \,/\Delta \text{x} \qquad m = Lk_\theta/2\pi \qquad (2)$$

where L = length of the poloidal cross-section of the magnetic flux surface. An example of the density phase spectrogram is presented in Figure 3.

6. AEs poloidal rotation velocity

Poloidally resolved density and potential measurements provide the frequency-poloidal wavenumber spectrum $S(k_\theta, f)$. An example of the mode evolution in density PSD is shown in Figure 4. The linear phase velocity of the AE is given by

$$V_{ExB}^{phase} = 2\pi f \,/\, k_\vartheta \qquad (3)$$

In the upper box of $S(k_\theta, f)$, $V_{ExB}^{phase} = 2\pi\ 188{\times}10^3 \,/\, 0.34$ [Hz cm] ~ $35{\times}10^3$ [m/s] = 35 [km/s]. The middle and the lower boxes give the same value for V_{ExB}^{phase}. The results, presented in the figure show the mode frequency evolution is associated with concordant k_θ evolution,

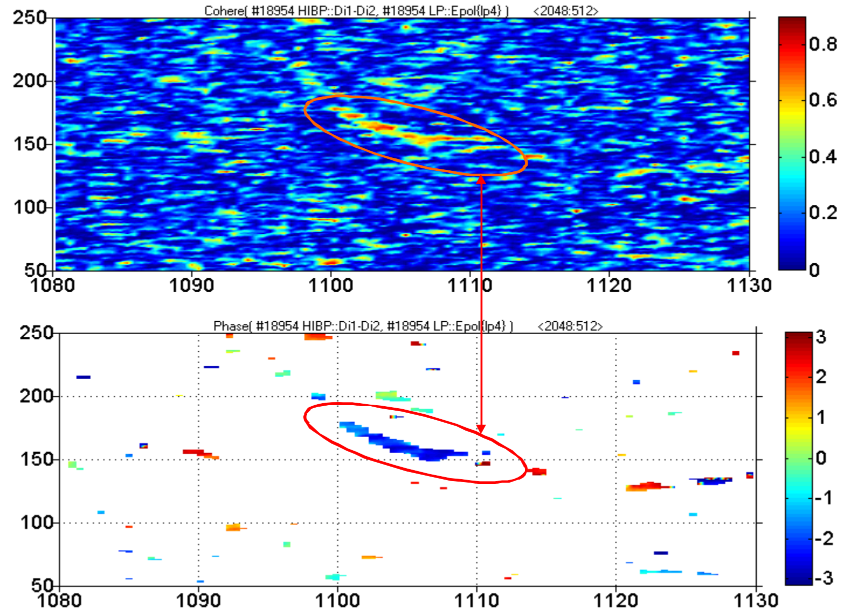

FIG. 2. Time evolution (spectrograms) of the $\{Coh_{EHIBP\ ELP'}(f,t)\}^2$ and cross-phase $\theta_{EHIBP\ ELP}$ between E_{HIBP} (ρ = 0.5) and E_{LP} (ρ = -0.9). The high $\{Coh^{AE}{}_{EHIBP\ ELP'}(f,\ t)\}^2 < 0.8$ long range (one half of plasma raduis) correlations are visible for the specific AE mode (t=1100-1110 ms).

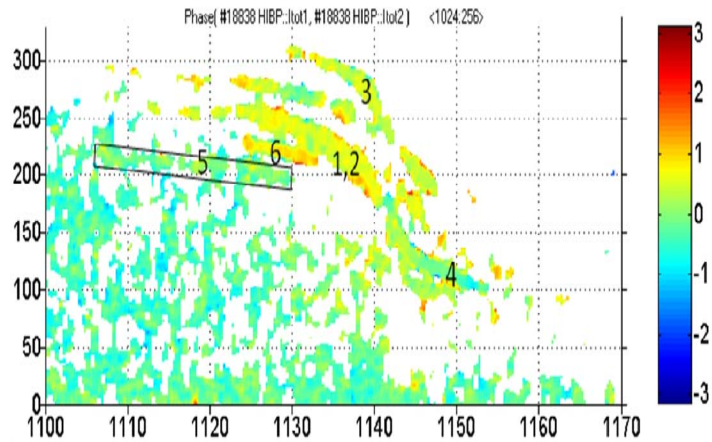

N	θ/π	*m*
1, 2	0.182 ± 0.05	4.55 ± 1.251
3	0.148 ± 0.07	3.7 ± 1.75
4	0.024 ± 0.09	0.6 ± 2.25
5	-0.03 ± 0.07	0.75 ± 1.75
6	0.26 ± 0.06	6.5 ± 1.5

FIG. 3. Time evolution (spectrograms) of the $\theta_{n1\ n2}$ - cross-phase between the densities, measured in two sample volumes (ρ = - 0.54). Only the points with high $Coh_{n1\ n2}$ (f, t) > 0.3 are shown in color. The color bar for the cross-phase is in radians. L = 83 cm, Δx = 1.66 cm.

providing the permanent V_{ExB}^{phase} . Figure 5 presents V_{ExB}^{phase} (*f, t*) spectrogram for the same shot. The positive sign of k_θ and V_{ExB}^{phase} imply propagation in the electron diamagnetic drift direction.

7. AE mode induced electrostatic particle flux

The AE contribution to the bulk plasma turbulent particle flux was studied in detail, following the method, described in [2]. Figure 6 presents the frequency resolved turbulent particle flux in the NBI sustained discharge. The flux related to the broadband turbulence has an intermittent character [6]. It consists of a stochastic sequence of spikes, mostly directed outward. AEs present quite pronounced quasi-coherent peaks in flux spectrograms.

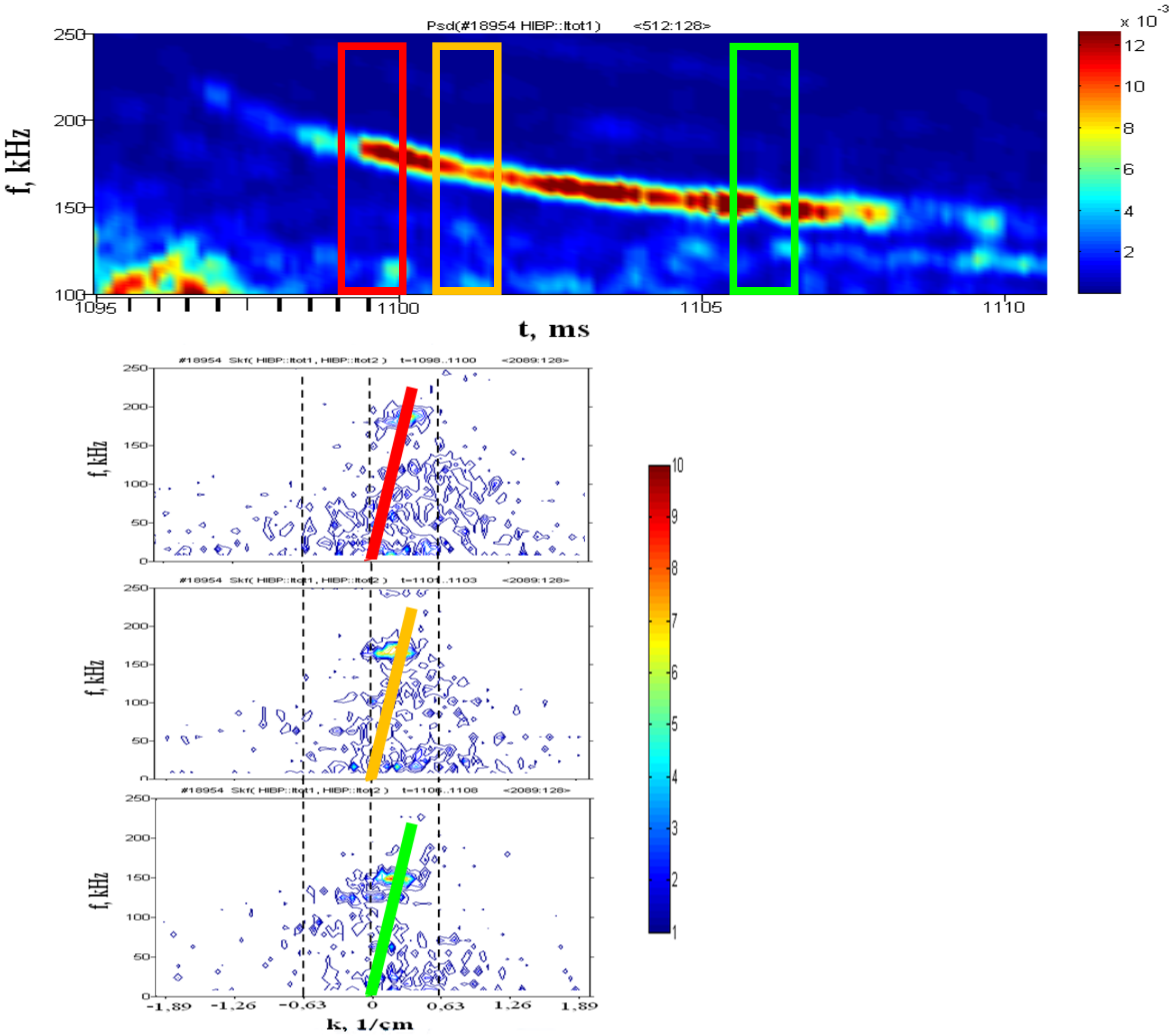

FIG. 4. HIBP density spectrogram (upper box) and frequency – wave-vector 2D density spectrum $S(k_\theta, f)$ for three time instants (ρ = -0.54).

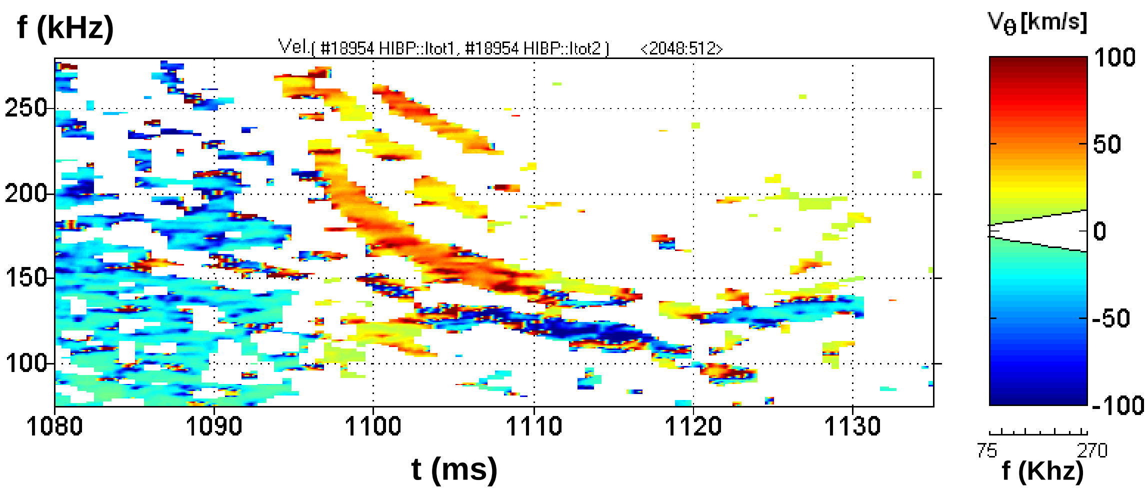

FIG. 5. V_{ExB}^{phase} (f, t) spectrogram for density perturbations. The color bar denotes the attainable velocity limit due to the finite Δx=1.66. (ρ = -0.54).

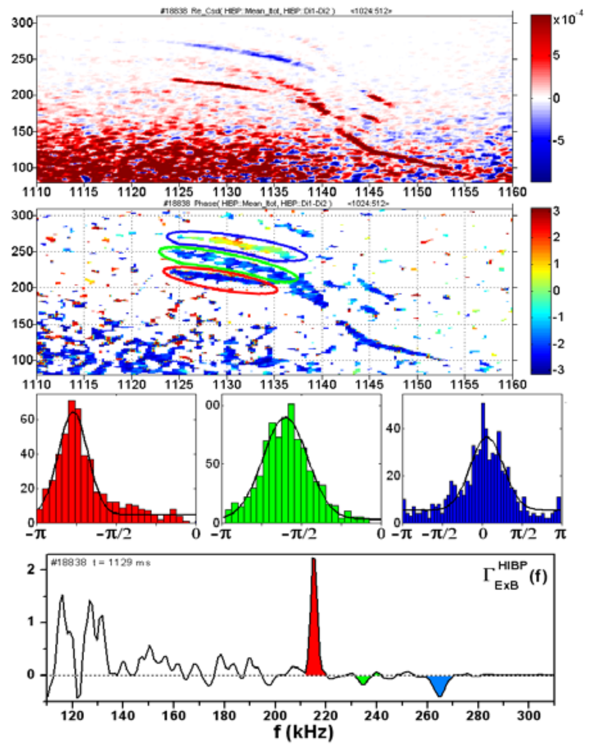

FIG. 6. a) Frequently resolved turbulent particle flux (in arb. units) in the NBI sustained discharge. Red color means outward flux, blue – inward flux. The AEs are quite visible in the spectrogram, indicating the AE contribution in the total turbulent flux is significant.
b) $\theta_{Epol\ ne}$ - Cross-phase between E_{pol} and n_e oscillations. Color bar is in radians. Three branches of the AE are marked by colored ovals.
c) The histograms of the cross-phase for each marked branches with corresponding colors. Left box – $\theta_{Epol\ ne} = -3/4\pi$, corresponding to the outward flux, central box $\theta_{Epol\ ne} = -\pi/2$, corresponding to zero flux, right box $\theta_{Epol\ ne} \sim 0$, corresponding to inward flux.
d) An example of the frequency spectrum of the turbulent particle flux, taken at some time instant, averaged over 1 ms. Three frequency peaks for the branches of the AE that are discussed have been marked with corresponding colors.

Figure 6 shows that AE modes may contribute to both outward and inward flux, and also produce no flux, depending on the phase relations between E_{pol} and density oscillations. Typically, $\Gamma^{AE}_{E\times B}$ - the AE contribution to the turbulent particle flux, was found to be a significant fraction of the total flux $\Gamma_{\mathrm{E\times B}}$. Figure 6 shows that $\Gamma^{AE}_{E\times B}$ exceeds the broadband turbulence flux $\Gamma^{BB}_{E\times B}$ from the same frequency domain.

8. MHD modelling for mode identification

Comparisons with computational MHD mode predictions indicate that some of the more prominent frequency lines can be identified with radially extended HAE (helical), GAE (global) and TAE (toroidal) modes [5]. The Alfvén mode structures have been calculated using the AE3D code [7], while the continuum structures are obtained from the STELLGAP code [8]. The AE3D model solves a reduced MHD set of shear Alfvén eigenmode equations using a Jacobi-Davidson method that allows one to efficiently search for eigenmodes within finite range frequency windows centered about a target frequency. The mode structure includes the effects of couplings from the 3D equilibrium and for both the continuum and eigenmode calculations. 9 toroidal modes were used to represent the eigenfunctions with the ranges of poloidal modes indicated in parentheses: $n = -1$ ($m = 0$-10), $n = -3$ ($m = 0$-10), $n = -5$ ($m = 0$-12), $n = -7$ ($m = 0$-12), $n = -9$ ($m = 0$-14), $n = -11$ ($m = 0$-18), $n = -13$ ($m = 0$-20), $n = -15$ ($m = 0$-25), $n = -17$ ($m = 0$-30).
An example is given in Fig. 7 of a mode that is observed experimentally at 257 kHz at t=1141, #18838. The full spectrograms are presented in Figure 1. In Figure 7(a) the $\theta_{n1\ n2}$ - cross-phase between n_{e} oscillations, observed in two poloidally shifted sample volumes, is presented. The Figure 7 (b) shows the histogram of the $\theta_{n1\ n2}$ for the presented branch, resulting in m = 3.7 ± 1.75. In Figure 7 (c) computed Alfvén continuum for this shot at t = 1140 ms is plotted, with the colors representing the dominant toroidal mode numbers. The radial mode structure of the mode-at the frequency 269.4 kHz marked by the black horizontal line is displayed in Fig. 7(d). Since this mode is dominated by coupling between m, n = (1, -1)

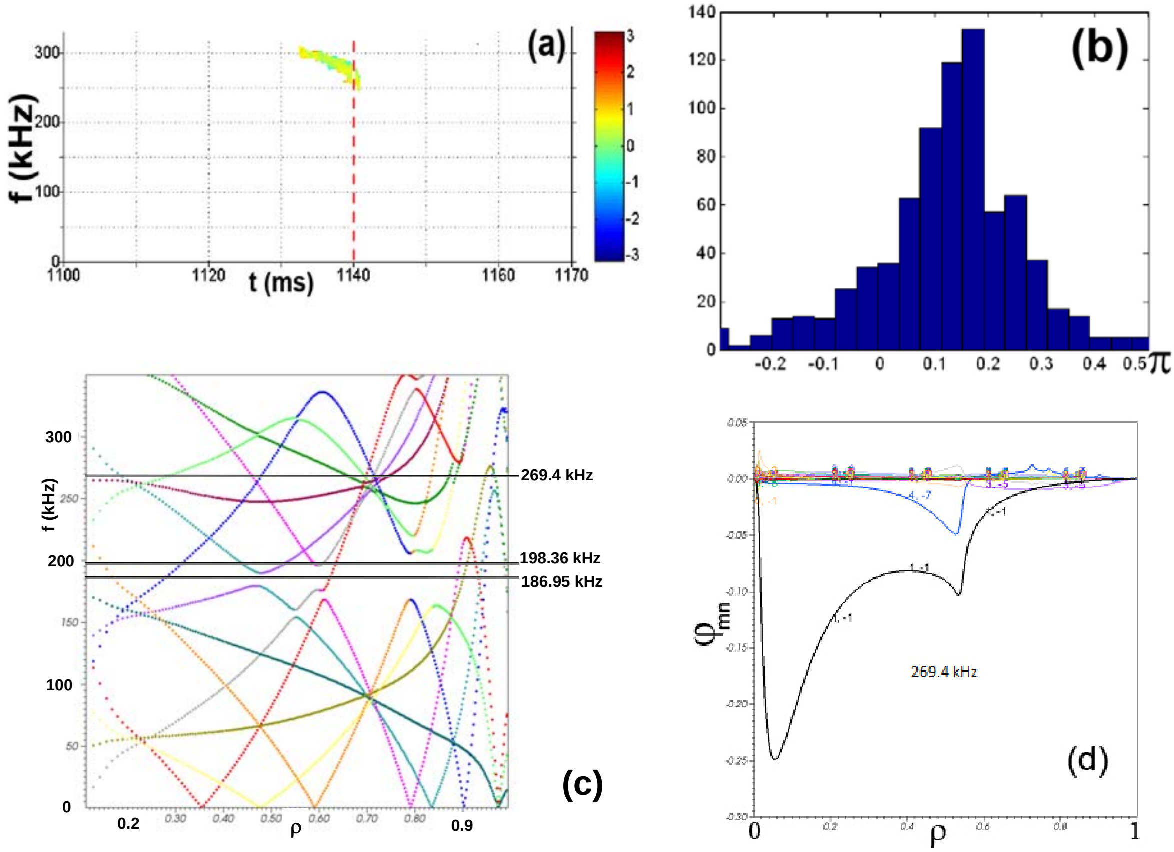

FIG. 7. #18838. (a) Spectrogram of $\theta_{n1\ n2}$ - cross-phase between n_e oscillations, observed in poloidally shifted sample volumes. Color bar is in radians. The only branch under study is presented; (b) the histogram of the $\theta_{n1\ n2}$ for the presented branch; $\theta/\pi = 0.148 + 0.07$, $m = 3.7 \pm 1.75$; (c) computed Alfvén continuum for this shot at t = 1140 ms with lines indicating several eigenmodes, (d) the mode structure at 269 kHz GAE/HAE mode (HAE character due to 1,-1/4,-7 coupling).

and (4,-7) components, it is classified as GAE/HAE. Finally the observed *m*=4 mode is identified as GAE/HAE mode. The next example is given in Fig. 8 of a couple of close modes that is observed in the same shot at 177 kHz and 181 kHz at *t*=1141 ms, marked in Fig 1 by the yellow circle. In Figure 8(a) the $\theta_{n1\ n2}$ –for this branch is presented. The Figure 8 (b) shows the histogram of the $\theta_{n1\ n2}$ for this branch, resulting in m = 4.55 ± 1.25. The radial mode structure of two closest modelled modes-at the frequencies 186.95 kHz and 193.36 kHz (marked by the black horizontal line is displayed in Fig. 7(c)), presented in Figure 8 (c) and (d). Both modes are identified as HAE modes since they both involve coupling of two dominant modes with differing m's and n's. Minor differences in frequency are expected due to effects of plasma flows and uncertainties in the plasma density and average ion mass.

9. Conclusions

The features and coherence characteristics of the NBI induced Alfven Eigenmodes were studied in the TJ-II heliac. Poloidal mode numbers and rotation velocities were measured. AEs present quite pronounced quasi-coherent peaks in the turbulent particle flux spectrograms. AEs may contribute to both outward and inward flux, and also produce no flux, depending on the phase relations between E_{pol} and density oscillations. Comparison with computational MHD mode predictions indicates that some of the more prominent frequency branches can be identified as radially extended HAE modes coupled to GAE modes.

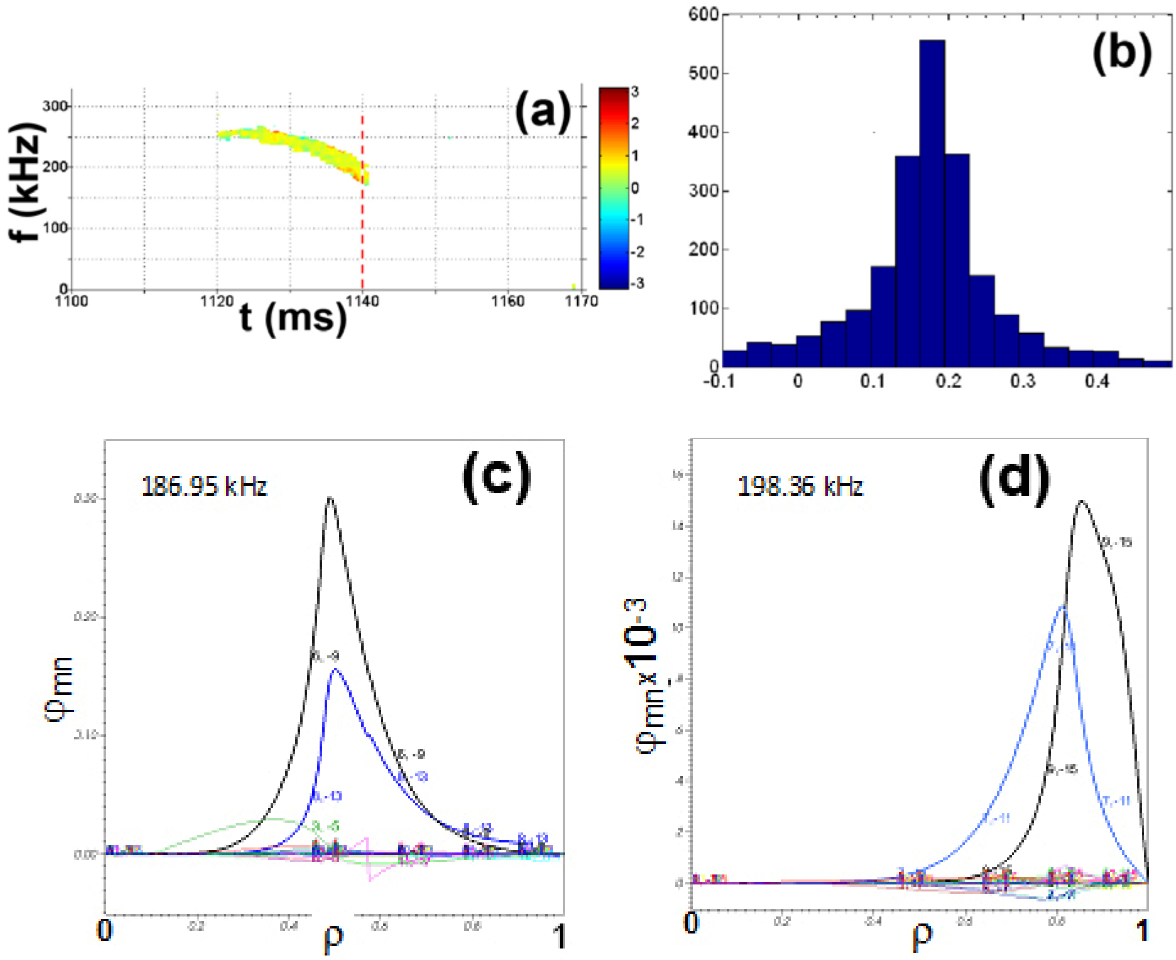

Fig. 8*. #18838. (a) Spectrogram of* $\theta_{n1\ n2}$ *for the branch under study. Color bar is in radians; (b) the histogram of the* $\theta_{n1\ n2}$ *for the presented branch;* $\theta/\pi = 0.182 \pm 0.05$*,* $m = 4.55 \pm 1.25$*; (c) the mode structure for t = 1140 ms at 186.95 kHz; (d) the mode structure t = 1140 ms at 198.36 kHz; m=6 mode is closest to experimental data.*

Acknowledgements

Authors are grateful to Prof. Yu.N. Dnestrovskij and Prof. K.A. Razumova for the continuous support of the activity of HIBP group and many valuable stimulating discussions.

The work of the Russian team was supported by RFBR 08-02-01326, 10-02-01385.

References

[1] JIMÉNEZ-GÓMEZ, R., et al., Nuclear Fusion, submitted.
[2] MELNIKOV, A., et al., Nuclear Fusion **50** (2010) 084023.
[3] MELNIKOV, A.V., et al., Fusion Sci. Technol. **51** (2007) 31.
[4] MELNIKOV, A.V., et al., 2009 Proc. 36-th EPS Conf. on Plasma Physics (Sofia, 2009) P-4.186, http://www.eps2009.uni-sofia.bg/
[5] MELNIKOV, A., et al., J. Fusion Research (2010), accepted.
[6] MELNIKOV, A.V., et al., 2010 Proc. 37-th EPS Conf. on Plasma Physics (Dublin, 2010) P1.066, http://osc.ciemat.es/EPS2010PAP/pdf/P1.066.pdf
[7] SPONG, D.A., D'AZEVEDO, E. AND TODO, Y., Phys. Plasmas **17** (2010) 022106.
[8] SPONG, D.A., SANCHEZ, R., AND WELLER, A., Phys. Plasmas **10 (**2003) 3217.